HHS Public Access

Author manuscript

Biochemistry. Author manuscript; available in PMC 2017 December 26.

Published in final edited form as:

Biochemistry. 2017 December 26; 56(51): 6652–6661. doi:10.1021/acs.biochem.7b01029.

Structural Characterization of Ferrous Ion Binding to Retinal Guanylate Cyclase Activator Protein-5 from Zebrafish Photoreceptors

Sunghyuk Lim[1], **Alexander Scholten**[2], **Grace Manchala**[1], **Diana Cudia**[1], **Sarah-Karina Zlomke-Sell**[2], **Karl-W. Koch**[2], and **James B. Ames**[1]

[1]Department of Chemistry, University of California, Davis, CA 95616

[2]Department of Biochemistry, University of Oldenburg, Germany

Abstract

Sensory guanylate cyclases (zGCs) in zebrafish photoreceptors are regulated by a family of guanylate cyclase activator proteins (called GCAP1-7). GCAP5 contains two non-conserved cysteine residues (Cys15 and Cys17) that could in principle bind to biologically active transition state metal ions (Zn^{2+} and Fe^{2+}). Here, we present nuclear magnetic resonance (NMR) and isothermal titration calorimetry (ITC) binding analysis that demonstrate the binding of one Fe^{2+} ion to two GCAP5 molecules (in a 1:2 complex) with a dissociation constant in the nanomolar range. At least one other Fe^{2+} binds to GCAP5 with micromolar affinity that likely represents electrostatic Fe^{2+} binding to the EF-hand loops. The GCAP5 double mutant (C15A/C17A) lacks nanomolar binding to Fe^{2+}, suggesting that Fe^{2+} at this site is ligated directly by thiolate groups of Cys15 and Cys17. Size exclusion chromatography analysis indicates that GCAP5 forms a dimer in both the Fe^{2+}-free and Fe^{2+}-bound states. NMR structural analysis and molecular docking studies suggest that a single Fe^{2+} ion is chelated by thiol side chains from Cys15 and Cys17 in the GCAP5 dimer, forming a $[Fe(SCys)_4]$ complex like that observed previously in two-iron superoxide reductases. Fe^{2+} binding to GCAP5 decreases its ability to activate photoreceptor human GC-E by decreasing GC-activity more than 10-fold. Our results indicate a strong Fe^{2+}-induced inhibition of GC by GCAP5 and suggest that GCAP5 may serve as a redox sensor in visual phototransduction.

Graphical abstract

Correspondence to: James B. Ames.

Conflict of Interest Disclosure. The authors declare no competing financial interest.

Supporting Information Available: Supporting information available online comprises 3 figures. This material is available free of charge via the Internet at http://pubs.acs.org.

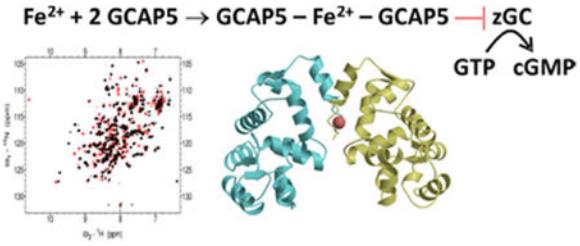

Introduction

Retinal guanylate cyclase activator proteins (GCAP1[1] and GCAP2[2]) were first identified as EF-hand calcium sensor proteins in mammalian photoreceptor rod and cone cells[3]. Both GCAP1 and GCAP2 control Ca^{2+}-sensitive activation of retinal guanylate cyclases (RetGCs[4, 5]) that is crucial for promoting the recovery phase of vertebrate visual phototransduction[6, 7]. Additional GCAP homologs were discovered recently in zebrafish (GCAP3-5 and 7[8]). *In situ* hybridization showed that expression of zebrafish specific GCs and GCAPs starts between 3 and 4 days post fertilization coinciding with the onset of visual function[9, 10]. Initial *in vitro* studies further demonstrated that GCAPs activate mammalian GCs in a step-by-step Ca^{2+}-relay mode fashion similar to the GC-GCAP system in mammals[11-13]. Interestingly, these earlier studies showed that GCAP5 is a much weaker GC activator compared to the other GCAPs under standard assay conditions[13]. Furthermore, GCAP5 has the most divergent amino acid sequence compared to mammalian and other zebrafish GCAP forms (Fig. 1). In particular, GCAP5 contains two non-conserved cysteine residues (Cys15 and Cys17) not found in the other GCAPs that in principle could be used to ligate biological transition metals such as Fe^{2+} and Zn^{2+}. Ferrous ion has been shown to serve as a redox sensor in a variety of cell types [14], and it is tempting to speculate that redox sensing by GCAP5 might control phototransduction in zebrafish photoreceptors. Indeed, the accumulation of iron levels in the retina have been correlated to age-related macular degeneration in humans, suggesting the involvement of redox-sensitive processes in the pathogenesis of the disease[15].

In the current study, we characterized both the structure and binding properties of Fe^{2+} binding to GCAP5 in zebrafish. Our ITC binding analysis demonstrates that one Fe^{2+} binds to two molecules of GCAP5 with nanomolar affinity, consistent with one Fe^{2+} bound per GCAP5 dimer. At least one additional Fe^{2+} binds to GCAP5 in the micromolar range that likely binds to the second EF-hand. NMR structural studies reveal that both Cys15 and Cys17 are essential for nanomolar Fe^{2+} binding to GCAP5, which form a $[Fe(SCys)_4]$ complex. Our functional studies indicate that Ca^{2+}-free/Fe^{2+}-bound and Ca^{2+}-bound/Fe^{2+}-bound GCAP5 both strongly inhibit mammalian GC activity compared to that of Fe^{2+}-free GCAP5. We suggest that Fe^{2+} levels in photoreceptors (and hence metabolic activity) may be controlled by light activation, and therefore propose that Fe^{2+} binding to GCAP5 may serve as a light-dependent redox sensor in zebrafish photoreceptors.

Materials and Methods

Cloning, expression and purification of GCAP5 forms

Recombinant myristoylated GCAP5 (hereafter designated as GCAP5) was used throughout this study and bacterial expression of myristoylated GCAP5 was accomplished by co-expressing the GCAP5 D3N mutant[16] and yeast N-myristoyl CoA transferase (NMT) in E. coli strain, BL21(DE3) as described previously[16] for GCAP1[17]. Acylation of the GCAP5 D3N mutant was originally confirmed in living cells by a click-chemistry approach[16]. Cloning of the C15A/C17A double mutant was similar as described for other point mutants of GCAPs[11, 13]. Accordingly, the double mutant was prepared employing primers 5′-CTCAGCGCCgcCAAAgcCCACCAGTGG-3′ (forward) and 5′-CTCGGTGGCGGACATGCTGG-3′ (reverse). Single point mutations were introduced to GCAP5 using the same reverse primer and 5′-CTCAGCGCCgcCAAATGCCACCAGTGG-3′ (forward) for the C15A mutant and 5′-CTCAGCGCCTGCAAAgcCCACCAGTGG-3′ (forward) for the C17A mutant. Purification of GCAP5 was achieved using previously described methods with the following modifications[18, 19]. Briefly, myristoylated GCAP5 was expressed in the soluble fraction, in contrast to unmyristoylated GCAP5 that was expressed in inclusion bodies. The cell lysate supernatant with the addition of 0.35 M NH_4SO_4 (final concentration) was loaded onto a Butyl sepharose column (HiPrep Butyl FF 16/10, GE Healthcare) equilibrated with loading buffer (20 mM Tris (pH7.5), 0.35M NH_4SO_4, and 1mM Dithiothreitol (DTT)), and the column was washed until the column wash contained no detectable protein ($A_{280} < 0.01$). GCAP5 protein (both wild type, $GCAP5^{WT}$ or C15A/C17A double mutant, $GCAP5^{C15A/C17A}$) was then eluted from the Butyl sepharose column with a low salt buffer (20 mM Tris (pH7.5), 2 mM ethylene glycol-bis(β-aminoethyl ether)-N,N,N′,N′-tetraacetic acid (EGTA) and 1 mM DTT). The eluted protein fraction from the Butyl-sepharose column was then diluted 5-fold and directly applied to a Q sepharose column (HiTrap 5ml Q HP, GE Healthcare) equilibrated in low salt buffer, and GCAP5 was eluted using a standard salt gradient[18, 19]. The eluted protein fraction from the Q-sepharose column was concentrated to a volume of 2 mL and then applied to a size exclusion chromatography column (HiLoad 26/600 Superdex, GE Healthcare) equilibrated in low salt buffer. The final GCAP5 protein was eluted into low salt buffer. Typically, 10 mg of final purified GCAP5 protein was obtained from 1 liter of cell culture. The final protein sample was more than 95% pure as judged by SDS-PAGE. Protein myristoylation was verified using reverse phase HPLC as described[20].

Analytical size exclusion chromatography (SEC)

Measurement of the molar mass of GCAP5 in the presence of Mg^{2+} (5 mM) and/or Fe^{2+} (1 mM) was performed using analytical SEC (Superdex 200 HR 10/30 column, GE Healthcare). A sample volume of 100 μL of GCAP5 (200 μM protein concentration) was applied to the column equilibrated with 30 mM MES (pH 6.6), 5 mM citrate, and 100 mM NaCl. The SEC measurements were made at 4 °C with a flow rate at 0.5 ml/min.

NMR spectroscopy

GCAP5 samples for NMR experiments consisted of ^{15}N-labeled myristoylated and Ca^{2+}-free GCAP5 (0.35 mM) dissolved in 30 mM MES (pH 6.6) buffer containing 1 mM DTT-d_{10} and 90%:10% H_2O:D_2O. To observe Fe^{2+} ion binding to GCAP5 by NMR, a series of samples of ^{15}N-labeled GCAP5^{WT} (and GCAP5$^{C15A/C17A}$) was prepared with the addition of 0, 0.25, 0.50, 1.0, 2.0, and 5.0 equivalents of $FeSO_4$ into the samples prepared anaerobically in a glove bag under constant purging with high purity argon gas. All NMR experiments were performed at 30°C on a Bruker 800 MHz Avance III spectrometer equipped with a triple resonance cryogenic TCI probe and pulsed field gradients. 2D ^{15}N-^{1}H HSQC with 2048 (^{1}H) × 256 (^{15}N) data points were acquired on ^{15}N-labeled GCAP1^{WT} or GCAP5$^{C15A/C17A}$ samples. Spectra were processed using NMRPipe software package[21] and analyzed using SPARKY[22].

Isothermal titration calorimetry (ITC)

Fe^{2+} binding to GCAP5^{WT} (and GCAP5$^{C15A/C17A}$) with ferrous gluconate was carried out on a VP-ITC calorimeter (Micro-Cal) at 25°C as described previously[23]. Metal free GCAP5 protein was prepared by first adding 5 mM EGTA into the protein sample (to remove contaminating Ca^{2+}) and residual EGTA was removed by performing repeated buffer exchange with Amicon spin concentrator. The ITC titration buffer contained 30 mM MES (pH 6.6), 100 mM NaCl, 2 mM ferrous gluconate, and 1 mM beta-mercaptoethanol. The concentration of GCAP5 in the titration was 50 μM and Fe^{2+} concentration in the titrant was 2 mM. The sample was titrated with 40 injections of 5 μl aliquots.

Molecular docking calculation

The web-based docking program HADDOCK[24] was used to generate a structural model of Fe^{2+}-bound to GCAP5. First, a homology modeled structure of monomeric GCAP5 was generated based on the crystal structure of chicken GCAP1 (PDB ID: 2R2I; 63% sequence identity) using Swiss-Modeler software[25]. This homology model of monomeric GCAP5 was then docked to a single Fe^{2+} using HADDOCK. For the Fe^{2+} docking, an unambiguous distance restraint between the bound Fe^{2+} ion and sulfur atoms of cysteine residues (Cys15 and Cys17) was set to 2.35 ±0.05 Å. This distance represents the average Fe-S bond length extracted from crystal structures of rubredoxin (PDB ID: 1FHM) and rubrerythrin (PDB ID: 1LKO). The docking calculation was initiated with a rigid body energy minimization that generated 1000 structures. The best 200 structures were subjected to a semi-flexible simulated annealing step. In the final step, the 200 structures obtained from the previous simulated annealing step were refined in explicit waters. The coordinate file with the lowest HADDOCK score was selected as the final model of Fe^{2+}-bound GCAP5. The structure of the GCAP5 dimer with one Fe^{2+} bound was built using HADDOCK, in which the Fe^{2+}-bound GCAP5 monomer (calculated above) was docked onto a second GCAP5 molecule. The same HADDOCK protocol above was used to dock the dimer. The distance between Fe^{2+} and each sulfur atom of the four cysteine residues in the dimer was set to 2.35 ± 0.05 Å. The distance between the four sulfur atoms in the dimer was set to 3.8 ± 0.1 Å, which matched the corresponding distances observed in the crystal structure of rubredoxin. At the end of the HADDOCK dimer calculation, 195 structures formed a single cluster out of 200

water-refined structures. The coordinate file with the lowest HADDOCK score was chosen for the final structural model displayed in this study.

Guanylate cyclase assays

For testing the regulatory properties of zGCAP5 and its mutant, we reconstituted purified GCAP5 forms with cell membranes containing heterologously expressed human GC-E in HEK flip 293 cells essentially as described previously[26, 27], but using a cell line that stably expressed GC-E. Cells were cultivated and harvested by centrifugation (300×g, 5 min), the supernatant was discarded and the pellet was resuspended in100 μL of 50 mM HEPES-KOH pH 7.4, 50 mM KCl, 20 mM NaCl, 1 mM DTT, mammalian protease inhibitor cocktail (1:500). Activities were measured according to a detailed protocol that was published before[13, 26] with the following modifications: GCAP5 and bovine GCAP1 (control) were added at a final concentration of 5 - 10 μM and Ca^{2+}-dependent GC activities were obtained by adjusting the free [Ca^{2+}] using a K_2H_2EGTA/CaH_2EGTA buffer system as described previously[13]. The free Mg^{2+}-concentration was 1 mM. For investigating the activity profile of Fe^{2+} bound GCAP5 we first resuspended lyophilized purified GCAP5 forms in 30 mM Mes buffer pH 6.6, 1 mM DTT. GCAP5 was saturated with Fe^{2+} by incubation with 100 μM Fe^{2+}, and unbound Fe^{2+} was removed by dialysis against 30 mM Mops pH 7.2, 60 mM KCl, 4 mM NaCl, 3.5 mM $MgCl_2$, 1 mM DTT, which kept Fe^{2+} at a minimum concentration of 100 nM ($FeSO_4$). Iron-loaded GCAP5 forms were reconstituted with recombinant GC-E and the activity was tested in the absence and presence of free Ca^{2+} in Mops-buffer (30mM) at pH 7.2, 60 mM KCl, 4 mM NaCl, 3.5 mM $MgCl_2$, 1 mM GTP, 0.3 mM ATP, 0.16 mM Zaprinast and 5 mM DTT. To avoid interference of the Ca^{2+}-chelating EGTA buffer with Fe^{2+}, we lowered the EGTA concentration to 50 μM in the assay mixture.

Results

Fe^{2+} binding to GCAP5 monitored by ITC

The binding of Fe^{2+} to GCAP5 was initially detected visually when highly concentrated and purified GCAP5 protein appeared to have a faint brownish or yellow color. Two non-conserved cysteine residues in GCAP5 (Cys15 and Cys17, see Fig. 1) were suggested to participate in Fe^{2+} binding, because the double mutation C15A/C17A in GCAP5 (called $GCAP5^{C15A/C17A}$) abolished the faint color. The UV-visible absorbance spectrum of iron-loaded GCAP5 exhibited two peaks at 325 nm and 420 nm indicative of the presence of an iron-sulfur cluster[28]. GCAP5 may also bind to Fe^{3+}, and the observed faint yellow color could also be due to light absorption by Fe^{3+}; however, Fe^{3+} binding to GCAP5 was not analyzed in this study, because Fe^{3+} under physiological conditions is not soluble enough for binding titrations by ITC or NMR.

Isothermal titration calorimetry (ITC) was used to quantitatively monitor Fe^{2+} binding to GCAP5 (Fig. 2). Titration of Fe^{2+} ions into wildtype GCAP5 (called $GCAP5^{WT}$) resulted in a binding isotherm that is multiphasic and could be fit by a two-site model with 2 or more Fe^{2+} ions (Figs. 2A-B). The binding isotherm in Fig. 2B exhibited two distinct phases: The first phase represents high affinity binding of Fe^{2+} (K_d < 100 nM) with a stoichiometry of 1 Fe^{2+} bound to two GCAP5 molecules (stoichiometric coefficient, n = 0.4 ±0.1). The

enthalpy change (ΔH) for the high affinity site could not be accurately measured due to confounding enthalpy changes caused by dissociation of Fe^{2+} complexes with gluconate and mercaptoethanol as well as redox dependent heat of dilution. The second phase in the binding isotherm represents exothermic binding of Fe^{2+} (ΔH = -2.8 ±0.1 kcal/mol) with a stoichiometry of at least 2 Fe^{2+} bound to each GCAP5 molecule (n = 2 ±0.5) and apparent dissociation constant in the micromolar range (K_d = 3 ±1 μM).

Titration of Fe^{2+} ions into the C15A/C17A double mutant ($GCAP5^{C15A/C17A}$) resulted in a monophasic exothermic binding isotherm that could be fit by a one-site model (Figs. 2C-D). The binding isotherm in Fig. 2D exhibited exothermic binding of Fe^{2+} (ΔH = -0.7 ±0.1 kcal/mol) with a dissociation constant in the micromolar range (K_d = 3 ±1 μM), but the amplitude of the exothermic heat signal was approximately six-fold lower. The double mutant ($GCAP5^{C15A/C17A}$) eliminated the nanomolar Fe^{2+} binding site observed for $GCAP5^{WT}$, suggesting that Cys15 and Cys17 are both essential for nanomolar Fe^{2+} binding to GCAP5. The micromolar Fe^{2+} binding observed for $GCAP5^{C15A/C17A}$ is possibly due to non-specific electrostatic interaction of Fe^{2+} with negatively charged EF-hand loops or negatively charged residues on the protein surface.

NMR titration of Fe^{2+} binding to GCAP5

To probe the structural effects of Fe^{2+} binding to GCAP5, ^{15}N-^{1}H HSQC NMR spectra were recorded for ^{15}N-labeled GCAP5 in the presence and absence of saturating Fe^{2+} concentration (Fig. 3). The HSQC spectrum of GCAP5 in the absence of Fe^{2+} (red peaks in Fig. 3) exhibits 191 well resolved peaks with uniform intensity, indicating that GCAP5 is stably folded under NMR conditions. Each peak in the HSQC spectrum represents a particular amide group with a unique chemical shift environment that provides a residue specific fingerprint of protein conformation. Thus, Fe^{2+}-dependent spectral changes in the HSQC can be analyzed to infer particular amino acids at or near the Fe^{2+} binding sites. The HSQC spectrum of GCAP5 in the presence of saturating levels of Fe^{2+} (black peaks in Fig. 3) revealed more than a dozen peaks whose spectral frequency and/or intensity were altered by the addition of Fe^{2+}. Fe^{2+}-binding caused some peaks to become broadened beyond detection (see peaks at 7.6, 7.8, 8.05, 9.1, 9.3, and 10.6 ppm), whereas Fe^{2+} also caused a few new peaks to appear (6.4, 6.8 and 9.7 ppm). The large number of Fe^{2+}-induced spectral changes suggests that GCAP5 has multiple Fe^{2+} binding sites, consistent with the Fe^{2+} binding heterogeneity observed in the ITC isotherm (Fig. 2B).

To discriminate the different Fe^{2+} binding sites, HSQC spectra of $GCAP5^{WT}$ (Fig. 4A) and $GCAP5^{C15A/C17A}$ (Fig. 4B) were recorded at many different Fe^{2+} concentrations. The NMR titration of $GCAP5^{WT}$ (Fig 4A) revealed two types of binding sites: one type had two separate resolved peaks that represent Fe^{2+}-free and Fe^{2+}-bound states (see magenta solid circle and arrows in Fig. 4A), which is indicative of slow exchange kinetics on the NMR chemical shift timescale. The term “slow exchange” in this context refers to Fe^{2+} binding event in which the exchange rate of binding is smaller (slower) than the frequency difference between the NMR peaks (representing the free and bound states). In other words, the exchange rate is slower than the chemical shift timescale and the two states are resolved. By contrast, many other peaks in the NMR titration exhibited fast exchange kinetics in which a

single peak titrates from the Fe^{2+}-free to Fe^{2+}-bound state (see magenta dashed circles in Fig. 4). In this case, the exchange rate is larger (faster) than the frequency difference between the free and bound peaks and the two states are not resolved. Instead, the two states are represented by a single averaged peak whose chemical shift titrates progressively from the Fe^{2+}-free to Fe^{2+}-bound state (see dashed circles in Fig. 4).

High affinity Fe^{2+} binding site

The Fe^{2+} binding site with slow exchange kinetics (and hence high affinity) is represented by sets of two NMR peaks in Fig. 4A that have different chemical shifts in the Fe^{2+}-free versus Fe^{2+}-bound states (see solid magenta circle and arrows in Fig. 4A). For example, the NMR peak in the Fe^{2+}-free state at 7.6/115 ppm is clearly resolved from its Fe^{2+}-bound resonance at 7.7/115 ppm (see solid magenta circle in Fig. 4A). During the NMR titration, the peak at 7.6/115 ppm (Fe^{2+}-free state) decreased in intensity as the Fe^{2+} concentration was increased, while the corresponding peak at 7.7/115 ppm (Fe^{2+}-bound state) increased in intensity as Fe^{2+} concentration was increased (Fig. 4C). A similar situation occurs for the NMR peak at 7.7/116 ppm in Fe^{2+}-free state that titrates into the peak at 6.8/117 ppm in the Fe^{2+}-bound state (see magenta arrows in Fig. 4A). The NMR intensity of each slow exchange peak (magenta circle and arrows in Fig. 4A) is plotted as a function of Fe^{2+} concentration (Fig. 4C). The concentration profiles in Fig. 4C indicate that the Fe^{2+}-bound peaks (7.7/115 ppm and 6.8/117 ppm) both saturate when the Fe^{2+}:GCAP5 ratio is 0.5, consistent with a binding stoichiometry in which one Fe^{2+} binds to two GCAP5 molecules. A similar 1:2 stoichiometry was observed for the high affinity Fe^{2+}-binding site detected by ITC (Fig. 2A-B).

The slow exchange peaks in the NMR titration of $GCAP5^{WT}$ in Fig. 4A (7.6/115 ppm and 7.7/116 ppm in Fe^{2+}-free state; vs 7.7/115 ppm and 6.8/117 ppm in Fe^{2+}-bound state) are not observed in the NMR titration of $GCAP5^{C15A/C17A}$ (Fig. 4B). The loss of these slow exchange peaks caused by the C15A/C17A mutation suggests that these peaks (7.6/115 ppm, 7.7/115 ppm, 7.7/116 ppm, and 6.8/117 ppm) are likely assigned to backbone amide resonances of Cys15 and Cys17 in the Fe^{2+}-free and Fe^{2+}-bound states, respectively. Thus, high affinity Fe^{2+} binding requires both Cys15 and Cys17, consistent with ITC observations above that indicate a lack of nanomolar Fe^{2+}-binding to $GCAP5^{C15A/C17A}$ (Fig. 2D).

Low affinity Fe^{2+} binding sites

A number of peaks in the NMR titration exhibited fast exchange kinetics, consistent with relatively low affinity Fe^{2+} binding (see dashed circles in Figs. 4A-B). The NMR peaks that titrate with fast exchange kinetics are present in NMR spectra of both $GCAP5^{WT}$ and $GCAP5^{C15A/C17A}$, and therefore represent bound Fe^{2+} that must be ligated by non-cysteine residues. These fast exchanging NMR peaks likely represent the multiple Fe^{2+} binding sites detected by ITC with micromolar affinity (Fig. 2). The multiple low affinity Fe^{2+} binding sites probed by NMR and ITC are likely due to non-specific electrostatic Fe^{2+} binding with negatively charged EF-hand loops. To test whether Fe^{2+} might be bound electrostatically to the EF-hand loops, we monitored Fe^{2+} binding to GCAP5 in the presence of saturating Ca^{2+} levels using ITC (Fig. S1). If Fe^{2+} binds electrostatically to EF-hand loops, then the presence of saturating Ca^{2+} should weaken or prevent Fe^{2+} binding to the EF-hand loops.

Ca^{2+} binds to two EF-hands of GCAP5 with nanomolar affinity (apparent K_D of 0.37 and 0.61 nM[16]) and to one EF-hand with an apparent K_D of 2.91 μM[16] compared to micromolar affinity for Fe^{2+}. The ITC Fe^{2+} binding isotherm in the presence of Ca^{2+} showed an overall lower ΔH (ΔH = -0.17 kcal/mol) for the exothermic Fe^{2+} binding phase (Fig. S1). Thus, the Ca^{2+}-induced lowering of ΔH is consistent with having Ca^{2+} bound to at least two EF-hands in GCAP5 that may impede Fe^{2+} binding to the EF-hands. Indeed, the most downfield NMR peak at 10.60 ppm (assigned to Gly68 in the second EF-hand, EF2) in the Fe^{2+}-free/Ca^{2+}-free/Mg^{2+}-free state undergoes a substantial Fe^{2+}-induced spectral shift upon adding a saturating amount of Fe^{2+} (Fig. 4D), consistent with possible Fe^{2+} binding at EF2. In the presence of physiological Mg^{2+} levels (1 mM), Mg^{2+} interferes with Ca^{2+}-binding to GCAP5[16] and is known to bind to EF2 in GCAP1[17,29]. To test whether Fe^{2+} can bind to EF2 in place of Mg^{2+}, an HSQC spectrum of Mg^{2+}-bound GCAP5 was recorded in the presence and absence of saturating Fe^{2+} (Fig. S2). In the absence of Fe^{2+}, the Mg^{2+}-bound GCAP5 exhibited a downfield peak at 10.65 ppm assigned to Gly68 that represents Mg^{2+} binding to EF2 like that observed for GCAP1[17]. This downfield peak becomes significantly broadened upon adding a saturating concentration of Fe^{2+}, consistent with Fe^{2+} binding to EF2 in place of Mg^{2+} when the Fe^{2+} concentration exceeds that of Mg^{2+}.

GCAP5 is a dimer

The molecular size of GCAP5 in solution was determined by size exclusion chromatography (SEC) in Fig. 5. The elution time of GCAP5, calibrated using protein standards (see black peaks in Fig. 5), corresponded to a molar mass of 40 kDa, indicating that GCAP5 is a dimer in solution. The addition of Fe^{2+} and/or Mg^{2+} had no effect on the GCAP5 elution time. Therefore, GCAP5 exists as a dimer in both the Fe^{2+}-free and Fe^{2+}-bound states. The addition of Ca^{2+} to GCAP5 caused a shorter elution time that corresponded to a molar mass of ~60 kDa. The Ca^{2+}-induced oligomerization of GCAP5 was also detected by NMR, and many NMR peaks of Ca^{2+}-bound GCAP5 were broadened beyond detection (Fig. S3). The Ca^{2+}-induced broadening of NMR peaks was also observed for unmyristoylated GCAP5, which argues against a possible Ca^{2+}-myristoyl switch for GCAP5[16].

Structural model of a GCAP5 dimer in a [$Fe(SCys)_4$] complex

The Fe^{2+} binding analysis by NMR and ITC above demonstrates that one Fe^{2+} binds with nanomolar affinity to two molecules of GCAP5. This high affinity Fe^{2+} binding to GCAP5 was abolished by the C15A/C17A mutation, suggesting that side-chain sulfur atoms may ligate the bound Fe^{2+}. A structural model of GCAP5 bound to Fe^{2+} was generated in a stepwise fashion. First, a three-dimensional homology model of GCAP5 was generated based on the known crystal structure of chicken GCAP1[30]. The homology modeled structure of GCAP5 was then docked (using HADDOCK, see Methods) to a single Fe^{2+} ion that was ligated directly to the thiolate atoms of Cys15 and Cys17 (Fig. 6A). In the structure of monomeric GCAP5 bound to Fe^{2+}, the indole side-chain of Trp20 is located in close proximity to the bound Fe^{2+}, which may explain the Fe^{2+}-induced NMR spectral shift of the Trp20 indole resonance at 9.7/127 ppm (Fig. 3). A bound Mg^{2+} at EF2 was included based on the downfield NMR resonance assigned to Gly68 of EF2 in the HSQC spectrum of Mg^{2+}-bound GCAP5 (Fig. S2).

To generate a dimeric structure of GCAP5, a second homology modeled structure of GCAP5 was docked onto the Fe^{2+}-bound GCAP5 structure in Fig. 6A. The modeled structure of the GCAP5 dimer (Fig. 6B) contains a single bound Fe^{2+} that is ligated by the four cysteinyl thiolates of Cys15 and Cys17 from the two docked GCAP5 molecules (Fig. 6B). In essence, a single bound Fe^{2+} bridges two GCAP5 molecules in a $[Fe(SCys)_4]$ complex (Fig. 6C).

Fe^{2+}-induced inhibition of guanylate cyclase

Fe^{2+}-binding to GCAP5 was unexpected and had not been observed for any other GCAP form before. Therefore, we asked, whether Fe^{2+}-bound GCAP5 differs from the Fe^{2+}-free form in its regulatory properties. Since we had to adjust the assay conditions for the addition of Fe^{2+}, we performed control incubations with bovine GCAP1 (well characterized under different assay conditions). GCAP5 is the weakest activator among all zebrafish GCAP forms showing only very low Ca^{2+}-dependent activation (x-fold is 1.5 in the case of nonmyristoylated GCAP5)[13]. In the absence of Fe^{2+}, GCAP5 activated recombinant human GC-E roughly by a factor of 20 at high and low Ca^{2+}-concentration when compared to the GC-activity in the absence of either GCAP5 or bovine GCAP1 (Figure 7). However, we did not see higher activity in the absence of Ca^{2+} as this is typically seen with other GCAP forms and in our control incubation using bovine GCAP1 (Figure 7B). Further, Fe^{2+}-bound GCAP5 strongly decreased GC-E activity independent of the absence or presence of Ca^{2+}. The GCAP5 double mutant C15A/C17A activated GC-E to a similar extent as the wildtype did. However, it showed a Ca^{2+}-dependent activation yielding an x-fold activation of 1.4 (Figure 7A). In the presence of Fe^{2+}, we observed a slight decrease in activity, but the Ca^{2+}-dependency was preserved (Figure 7A). In contrast, the presence of Fe^{2+} decreased the activation of GC-E by Ca^{2+}-free GCAP1 reaching the same level as with Ca^{2+}-bound GCAP1 (Figure 7B). Fe^{2+} did not influence GC-E activity in the absence of any GCAP (Figure 7C).

Discussion

We present ITC (Fig. 2), NMR (Figs. 3-4) and cyclase enzymatic assays (Fig. 7) that monitor and structurally characterize Fe^{2+} binding to GCAP5. One Fe^{2+} binds to two molecules of GCAP5 with nanomolar affinity, and additional Fe^{2+} ions bind to GCAP5 with micromolar affinity. The low affinity Fe^{2+} binding to EF2 (Fig. 4D) is likely not physiological, because micromolar Fe^{2+} levels are outside the physiological range. The highest affinity Fe^{2+} binding site is not observed in the $GCAP5^{C15A/C17A}$ mutant (Figs. 2B and 4B), consistent with the bound Fe^{2+} at this site being ligated by side-chain sulfur atoms in Cys15 and Cys17. A structural model of a GCAP5 dimer forming a $[Fe(SCys)_4]$ complex (Figs. 6B) shows a single bound Fe^{2+} ligated by the four sulfur atoms from Cys15 and Cys17 in a symmetric dimer (Fig. 6E). A similar $[Fe(SCys)_4]$ structural motif was reported previously in the crystal structures of rubredoxin[31] (Fig. 6E, right panel) and a two-iron superoxide reductase[32, 33]. Our SEC data on GCAP5 (Fig. 5) indicate that both Fe^{2+}-free and Fe^{2+}-bound GCAP5 exist as a dimer in solution. A structural model of the Fe^{2+}-bound GCAP5 dimer (Fig. 6B) suggests intermolecular protein hydrophobic contacts (between His18 and Val76) as well as an intermolecular hydrogen bond (between Lys84 and Gln88) that may stabilize GCAP5 as a pre-formed protein dimer in the Fe^{2+}-free state (Fig. 6D).

The intermolecular contact involving Val76 was also implicated in the dimerization of GCAP1, because mutating this Val residue to Glu abolishes dimerization of GCAP1[17, 19, 34].

The bound Fe^{2+} in GCAP5 is coordinated by four cysteinyl thiolate atoms (Fig. 6E) that is quite similar to the structure of a bound Zn^{2+} in a Cys4 zinc finger motif[35]. This structural similarity suggests that Zn^{2+} might bind to GCAP5 in place of Fe^{2+} at the high affinity site. Zn^{2+} is transported into retinal photoreceptor cells and has been suggested to play a role in phototransduction[36]. Future studies are needed to probe whether Zn^{2+} can replace Fe^{2+} and bind with nanomolar affinity to GCAP5. If so, then it will be interesting to test whether Zn^{2+} binding to GCAP5 (like Fe^{2+} binding) can also regulate zGCs during visual phototransduction.

Functional implications of Fe^{2+}-binding to GCAP5

Our results suggest that Fe^{2+} binding to GCAP5 may stabilize and perhaps modulate the quaternary structure of the GCAP5 dimer that could play a role in regulating zebrafish GCs. However, our *in vitro* functional analysis in this study employed a recombinant mammalian GC, since active recombinant photoreceptor specific GCs from zebrafish are not currently available. Although zebrafish GCAP5 can regulate native zebrafish GCs in retinae membranes[9], we currently do not have access to zebrafish GC samples in live animals. The addition of Fe^{2+} caused complex effects on the regulation of mammalian GC and showed a strong inhibitory effect mediated by both GCAP5 and GCAP1 (Figs. 7A and 7B). The Fe^{2+}-induced GC inhibition meditated by GCAP1 is surprising, and might indicate possible Fe^{2+} binding to the EF-hands in GCAP1 that may mimick Ca^{2+} binding. The Fe^{2+}-induced inhibition of GC was somewhat weakened by the GCAP5 double mutant (C15A/C17A), consistent with functional Fe^{2+} binding by Cys15 and Cys17 (Fig. 6). The GCAP5 double mutant also showed a more typical Ca^{2+}-dependent activation of the target GC compared to the Ca^{2+}-independent GC activation by $GCAP5^{WT}$ (Fig. 7A). This suggests that Fe^{2+} binding to GCAP5 may stabilize the inhibitory conformational state of GCAP5 even in the absence of Ca^{2+}, and therefore Fe^{2+}-bound GCAP5 may serve to constitutively disable GC activation. The lack of Ca^{2+}-sensitive GC activation by $GCAP5^{WT}$ might also be explained by differences in our test incubations when compared to previous results[9, 13]. In the current study, we used myristoylated GCAP5 instead of nonmyristoylated protein that was used previously. The presence of the myristoyl group in GCAP5 appears to prevent the typical Ca^{2+}-sensitive activation of a GC, whereas the double mutation (C15A/C17A) restored the Ca^{2+}-dependent GC activation. These observations suggest a complex interdependence of the Fe^{2+} binding site (at Cys15 and Cys17), the myristoyl group, and the Ca^{2+}-free/Mg^{2+}-bound activator state of GCAP5. The source of GC in our test system was not critical for the outcome of the assay. We compared heterologously expressed human GC-E in HEK 293 cells with mammalian GC from native bovine rod outer segment membranes and did not observe a principal difference in the results (data not shown).

Does Fe^{2+}-binding to GCAP5 have any physiological meaning? At this point, we can only speculate on possible physiological implications, but several observations suggest that GCAP5 might not be the main activator of GCs in the zebrafish retina. Indeed, all other zebrafish GCAPs are at least 3-fold more active than GCAP5[13]. Furthermore, the expression

and activation profiles of the other GCAPs promote a dynamic Ca^{2+}-sensitive activation of zebrafish GCs in the absence of GCAP5, suggesting a lack of GCAP5 participation perhaps due to compensatory actions[9-13]. Finally, the downregulation of GCAP5 by Fe^{2+} further diminishes the already weak impact of GCAP5 on GC activation. Instead, we suggest that GCAP5 might bind to a different and as yet unknown target protein. Preliminary studies suggest that GCAP5 is expressed in the inner segment (K.W.K and A.S., unpublished results). Therefore, the binding of Fe^{2+} to GCAP5 might serve a regulatory role for a redox-sensitive process in the inner segment. Future experiments are needed to look for a GCAP5 binding partner protein expressed in the inner segment.

The Fe^{2+}-induced inhibition of GC mediated by GCAP5 (Fig. 7A) may protect photoreceptor cells from apoptosis and possibly prevent retinal degeneration. Mutations in GCs and/or GCAPs that cause constitutive GC activation are genetically linked to retinal degeneration[29, 37-41]. Also, the retinal degeneration 3 (RD3) protein (that binds to GC in place of GCAPs and prevents GC activation) is important for turning off basal cyclase activity during the trafficking of GC to the outer segment[42]. The basal cyclase activity of GC that occurs in the absence of RD3 is thought to trigger apoptosis of photoreceptor cells that could lead to retinal degeneration[43]. Therefore, inhibition of basal cyclase activity by RD3 is believed to be important for preventing retinal degeneration. We suggest that Fe^{2+}-induced inhibition of GC by GCAP5 might be a different mechanism for turning off GC activity in the inner segment, which could serve to protect zebrafish photoreceptor cells from retinal degeneration.

Supplementary Material

Refer to Web version on PubMed Central for supplementary material.

Acknowledgments

We thank Bennett Addison for help with NMR experiments.

†This work was supported by a grant from the National Institutes of Health (EY012347 to J.B.A. and by grants from the Deutsche Forschungsgemeinschaft, KO948/7-2 to K.W.K and GRK1885/1 to K.W.K and to the Research Training Group in Oldenburg).

References

1. Palczewski K, Subbaraya I, Gorczyca WA, Helekar BS, Ruiz CC, Ohguro H, Huang J, Zhao X, Crabb JW, Johnson RS. Molecular cloning and characterization of retinal photoreceptor guanylyl cyclase-activating protein. Neuron. 1994; 13:395–404. [PubMed: 7520254]
2. Dizhoor AM, Olshevskaya EV, Henzel WJ, Wong SC, Stults JT, Ankoudinova I, Hurley JB. Cloning, sequencing and expression of a 24-kDa Ca2+-binding protein activating photoreceptor guanylyl cyclase. J Biol Chem. 1995; 270:25200–25206. [PubMed: 7559656]
3. Palczewski K, Polans AS, Baehr W, Ames JB. Ca(2+)-binding proteins in the retina: structure, function, and the etiology of human visual diseases. Bioessays. 2000; 22:337–350. [PubMed: 10723031]
4. Dizhoor AM, Lowe DG, Olsevskaya EV, Laura RP, Hurley JB. The human photoreceptor membrane guanylyl cyclase, RetGC, is present in outer segments and is regulated by calcium and a soluble activator. Neuron. 1994; 12:1345–1352. [PubMed: 7912093]

5. Lowe DG, Dizhoor AM, Liu K, Gu Q, Spencer M, Laura R, Lu L, Hurley JB. Cloning and expression of a second photoreceptor-specific membrane retina guanylyl cyclase (RetGC), RetGC-2. Proc Natl Acad Sci USA. 1995; 6:5535–5539.
6. Koch KW, Duda T, Sharma RK. Photoreceptor specific guanylate cyclases in vertebrate phototransduction. Mol Cell Biochem. 2002; 230:97–106. [PubMed: 11952100]
7. Koch KW, Stryer L. Highly cooperative feedback control of retinal rod guanylate cyclase by calcium ions. Nature. 1988; 334:64–66. [PubMed: 2455233]
8. Imanishi Y, Yang L, Sokal I, Filipek S, Palczewski K, Baehr W. Diversity of guanylate cyclase-activating proteins (GCAPs) in teleost fish: characterization of three novel GCAPs (GCAP4, GCAP5, GCAP7) from zebrafish (Danio rerio) and prediction of eight GCAPs (GCAP18) in pufferfish (Fugu rubripes). J Mol Evol. 2004; 59:204–217. [PubMed: 15486694]
9. Fries R, Scholten A, Saftel W, Koch KW. Zebrafish guanylate cyclase type 3 signaling in cone photoreceptors. PLoS One. 2013; 8:e69656. [PubMed: 23940527]
10. Ratscho N, Scholten A, Koch KW. Expression profiles of three novel sensory guanylate cyclases and guanylate cyclase-activating proteins in the zebrafish retina. Biochim Biophys Acta. 2009; 1793:1110–1114. [PubMed: 19168097]
11. Fries R, Scholten A, Saftel W, Koch KW. Operation profile of zebrafish guanylate cyclase-activating protein 3. Journal of neurochemistry. 2012; 121:54–65. [PubMed: 22212098]
12. Koch KW. The guanylate cyclase signaling system in zebrafish photoreceptors. FEBS J. 2013; 587:2055–2059.
13. Scholten A, Koch KW. Differential calcium signaling by cone specific guanylate cyclase-activating proteins from the zebrafish retina. PLoS One. 2011; 6:e23117. [PubMed: 21829700]
14. Crack JC, Green J, Thomson AJ, Le Brun NE. Iron-sulfur clusters as biological sensors: the chemistry of reactions with molecular oxygen and nitric oxide. Accounts of chemical research. 2014; 47:3196–3205. [PubMed: 25262769]
15. Sterling J, Guttha S, Song Y, Song D, Hadziahmetovic M, Dunaief JL. Iron importers Zip8 and Zip14 are expressed in retina and regulated by retinal iron levels. Experimental eye research. 2017; 155:15–23. [PubMed: 28057442]
16. Sulmann S, Vocke F, Scholten A, Koch KW. Retina specific GCAPs in zebrafish acquire functional selectivity in Ca2+-sensing by myristoylation and Mg2+-binding. Scientific reports. 2015; 5:11228. [PubMed: 26061947]
17. Lim S, Peshenko IV, Olshevskaya EV, Dizhoor AM, Ames JB. Structure of Guanylyl Cyclase Activator Protein 1 (GCAP1) Mutant V77E in a Ca2+-free/Mg2+-bound Activator State. J Biol Chem. 2016; 291:4429–4441. [PubMed: 26703466]
18. Lim S, Peshenko IV, Dizhoor AM, Ames JB. Effects of Ca2+, Mg2+, and myristoylation on guanylyl cyclase activating protein 1 structure and stability. Biochemistry. 2009; 48:850–862. [PubMed: 19143494]
19. Lim S, Peshenko IV, Dizhoor AM, Ames JB. Structural insights for activation of retinal guanylate cyclase by GCAP1. PLoS One. 2013; 8:e81822. [PubMed: 24236217]
20. Dizhoor AM, Ericsson LH, Johnson RS, Kumar S, Olshevskaya E, Zozulya S, Neubert TA, Stryer L, Hurley JB, Walsh KA. The NH2 terminus of retinal recoverin is acylated by a small family of fatty acids. J Biol Chem. 1992; 267:16033–16036. [PubMed: 1386601]
21. Delaglio F, Grzesiek S, Vuister GW, Zhu G, Pfeiffer J, Bax A. NMRPipe: a multidimensional spectral processing system based on UNIX pipes. J Biomol NMR. 1995; 6:277–293. [PubMed: 8520220]
22. Lee W, Tonelli M, Markley JL. NMRFAM-SPARKY: enhanced software for biomolecular NMR spectroscopy. Bioinformatics. 2015; 31:1325–1327. [PubMed: 25505092]
23. Wingard JN, Chan J, Bosanac I, Haeseleer F, Palczewski K, Ikura M, Ames JB. Structural analysis of Mg2+ and Ca2+ binding to CaBP1, a neuron-specific regulator of calcium channels. J Biol Chem. 2005; 280:37461–37470. [PubMed: 16147998]
24. van Zundert GC, Rodrigues JP, Trellet M, Schmitz C, Kastritis PL, Karaca E, Melquiond AS, van Dijk M, de Vries SJ, Bonvin AM. The HADDOCK2.2 Web Server: User-Friendly Integrative Modeling of Biomolecular Complexes. Journal of molecular biology. 2016; 428:720–725. [PubMed: 26410586]

25. Arnold K, Bordoli L, Kopp J, Schwede T. The SWISS-MODEL workspace: a web-based environment for protein structure homology modelling. Bioinformatics. 2006; 22:195–201. [PubMed: 16301204]
26. Koch, KW., Helten, A. Signal Transduction in the Retina. Taylor and Francis CRC Press; 2008. Guanylate cyclase-based signaling in photoreceptors and retina; p. 121-143.
27. Zagel P, Dell'Orco D, Koch KW. The dimerization domain in outer segment guanylate cyclase is a Ca(2)(+)-sensitive control switch module. Biochemistry. 2013; 52:5065–5074. [PubMed: 23815670]
28. Huang Q, Hong X, Hao Q. SNAP-25 is also an iron-sulfur protein. FEBS letters. 2008; 582:1431–1436. [PubMed: 18375205]
29. Marino V, Sulmann S, Koch KW, Dell'Orco D. Structural effects of Mg(2)(+) on the regulatory states of three neuronal calcium sensors operating in vertebrate phototransduction. Biochim Biophys Acta. 2015; 1853:2055–2065. [PubMed: 25447547]
30. Stephen R, Bereta G, Golczak M, Palczewski K, Sousa MC. Stabilizing function for myristoyl group revealed by the crystal structure of a neuronal calcium sensor, guanylate cyclase-activating protein 1. Structure. 2007; 15:1392–1402. [PubMed: 17997965]
31. Min T, Ergenekan C, Eidsness M, Ichiye T, Kang C. Leucine 41 is a gate for water entry in the reduction of Clostridium pasteurianum rubredoxin. Protein science: a publication of the Protein Society. 2001; 10:613–621. [PubMed: 11344329]
32. deMaré F, Kurtz D, Nordlund P. The structure of Desulfovibrio vulgaris rubrerythrin reveals a unique combination of rubredoxin-like FeS4 and ferritin-like diiron domains. Nat Struct Biol. 1996; 3:539–546. [PubMed: 8646540]
33. Emerson JP, Cabelli DE, Kurtz DM Jr. An engineered two-iron superoxide reductase lacking the [Fe(SCys)4] site retains its catalytic properties in vitro and in vivo. Proceedings of the National Academy of Sciences of the United States of America. 2003; 100:3802–3807. [PubMed: 12637682]
34. Peshenko IV, Olshevskaya EV, Lim S, Ames JB, Dizhoor AM. Identification of target binding site in photoreceptor guanylyl cyclase-activating protein 1 (GCAP1). J Biol Chem. 2014; 289:10140–10154. [PubMed: 24567338]
35. Tang Q, Liu YP, Yan XX, Liang DC. Structural and functional characterization of Cys4 zinc finger motif in the recombination mediator protein RecR. DNA repair. 2014; 24:10–14. [PubMed: 25460918]
36. Redenti S, Ripps H, Chappell RL. Zinc release at the synaptic terminals of rod photoreceptors. Experimental eye research. 2007; 85:580–584. [PubMed: 17825289]
37. Jiang L, Baehr W. GCAP1 Mutations Associated with Autosomal Dominant Cone Dystrophy. Adv Exp Med Biol. 2010; 664:273–282. [PubMed: 20238026]
38. Payne AM, Downes SM, Bessant DA, Taylor R, Holder GE, Warren MJ, Bird AC, Bhattacharya SS. A mutation in guanylate cyclase activator 1A (GUCA1A) in an autosomal dominant cone dystrophy pedigree mapping to a new locus on chromosome 6p21.1. Hum Mol Genetics. 1998; 7:273–277.
39. Koch KW, Dell'Orco D. Protein and Signaling Networks in Vertebrate Photoreceptor Cells. Frontiers in molecular neuroscience. 2015; 8:67. [PubMed: 26635520]
40. Dell'Orco D, Sulmann S, Zagel P, Marino V, Koch KW. Impact of cone dystrophy-related mutations in GCAP1 on a kinetic model of phototransduction. Cell Mol Life Sci. 2014; 71:3829–3840. [PubMed: 24566882]
41. Kitiratschky VBD, Behnen P, Kellner U, Heckenlively JR, Zrenner E, Jägle H, Kohl S, Wissinger B, Koch KW. Mutations in the GUCA1A gene involved in hereditary cone dystrophies impair calcium-mediated regulation of guanlyate cyclase. Hum Mutat. 2009; 30:E782–796. [PubMed: 19459154]
42. Zulliger R, Naash MI, Rajala RV, Molday RS, Azadi S. Impaired association of retinal degeneration-3 with guanylate cyclase-1 and guanylate cyclase-activating protein-1 leads to congenital amaurosis-1. J Biol Chem. 2015; 290:3488–3499. [PubMed: 25477517]

43. Peshenko IV, Olshevskaya EV, Dizhoor AM. Functional Study and Mapping Sites for Interaction with the Target Enzyme in Retinal Degeneration 3 (RD3) Protein. J Biol Chem. 2016; 291:19713–19723. [PubMed: 27471269]

Abbreviations

EGTA	ethylene glycol-bis(β-aminoethyl ether)-N,N,N′,N′-tetraacetic acid
HSQC	heteronuclear single quantum coherence
ITC	isothermal titration calorimetry
NMR	nuclear magnetic resonance
GC	retinal guanylate cyclase
SEC	size exclusion chromatography

Figure 1. Amino acid sequence alignment of GCAP proteins

EF-hand motifs are shaded in color (EF1 green, EF2 red, EF3 cyan and EF4 yellow). Non-conserved cysteine residues (Cys15 and Cys17) in GCAP5 are highlighted in bold and red. Swiss Protein Database accession numbers are Q90WX4 (zebrafish GCAP1), Q90WX3 (zebrafish GCAP2), Q8UUX9 (zebrafish GCAP3), Q6ZM98 (zebrafish GCAP4), and Q5MAC8 (zebrafish GCAP5).

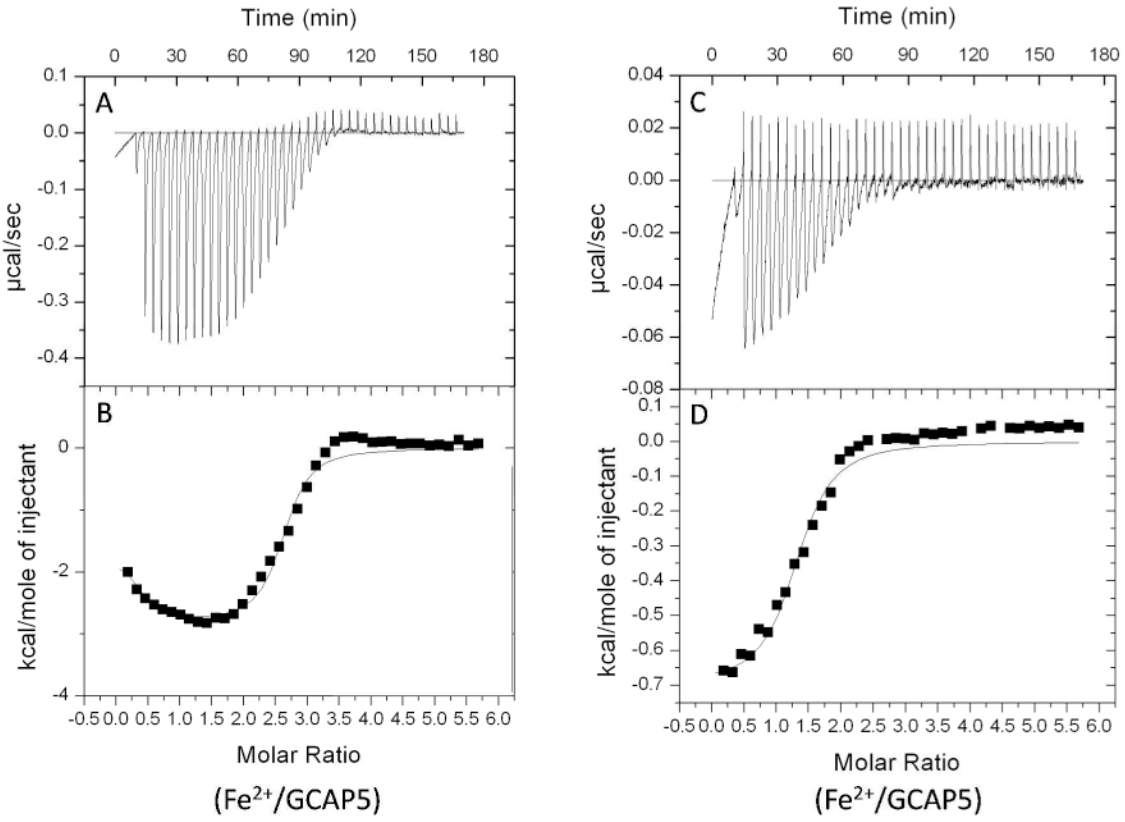

Figure 2. GCAP5 binds to Fe $^{+}$ as measured by ITC

Change of heat resulting from incremental addition of Fe^{2+} to $GCAP5^{WT}$ (A) or $GCAP5^{C15A/C17A}$ (C) during ITC titration at 25°C. Binding isotherms of Fe^{2+} binding to $GCAP5^{WT}$ (B) or $GCAP5^{C15A/C17A}$ (D) were derived from the integrated heat at each injection. The binding isotherm for $GCAP5^{WT}$ (B) was fit to a two-site model (see Methods). The fit suggests a high affinity site with a dissociation constant (K_d) that is less than 100 nM and stoichiometry (n) equal to 0.4 ±0.1 equivalents of Fe^{2+} bound per GCAP5 polypeptide. The lower affinity site has an apparent K_d of 3 ±1 µM with a stoichiometric coefficient of 2 ±0.5 and ΔH = -2.8 ±0.1 kcal/mol. The binding isotherm for $GCAP5^{C15A/C17A}$ (D) was fit to a onesite model with dissociation constant of 3 ±1 µ M and ΔH = -0.7 ±0.1 kcal/mol.

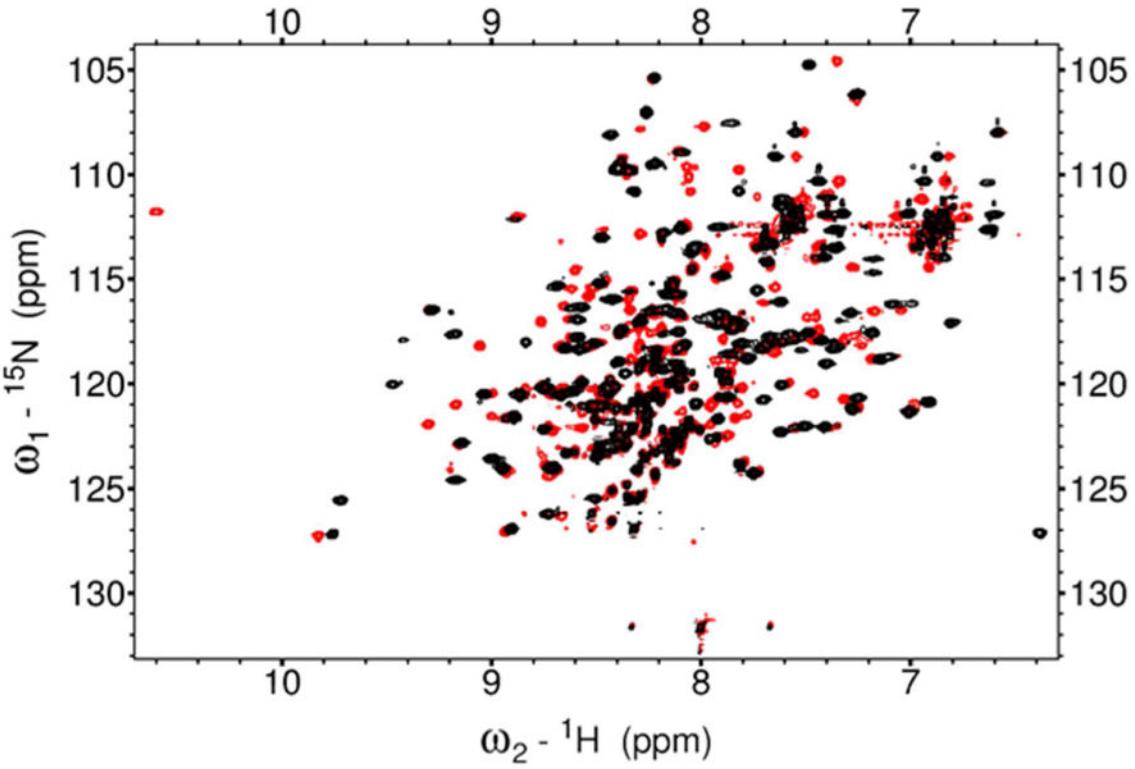

Figure 3. NMR spectroscopy of GCAP5 vs Fe^{2+}

^{1}H-^{15}N HSQC spectra of ^{15}N-labeled GCAP5 in the Fe^{2+}-free (red) and Fe^{2+}-saturated (black) states. The experimental conditions are defined under Materials and Methods and were the same as described previously for GCAP1[17].

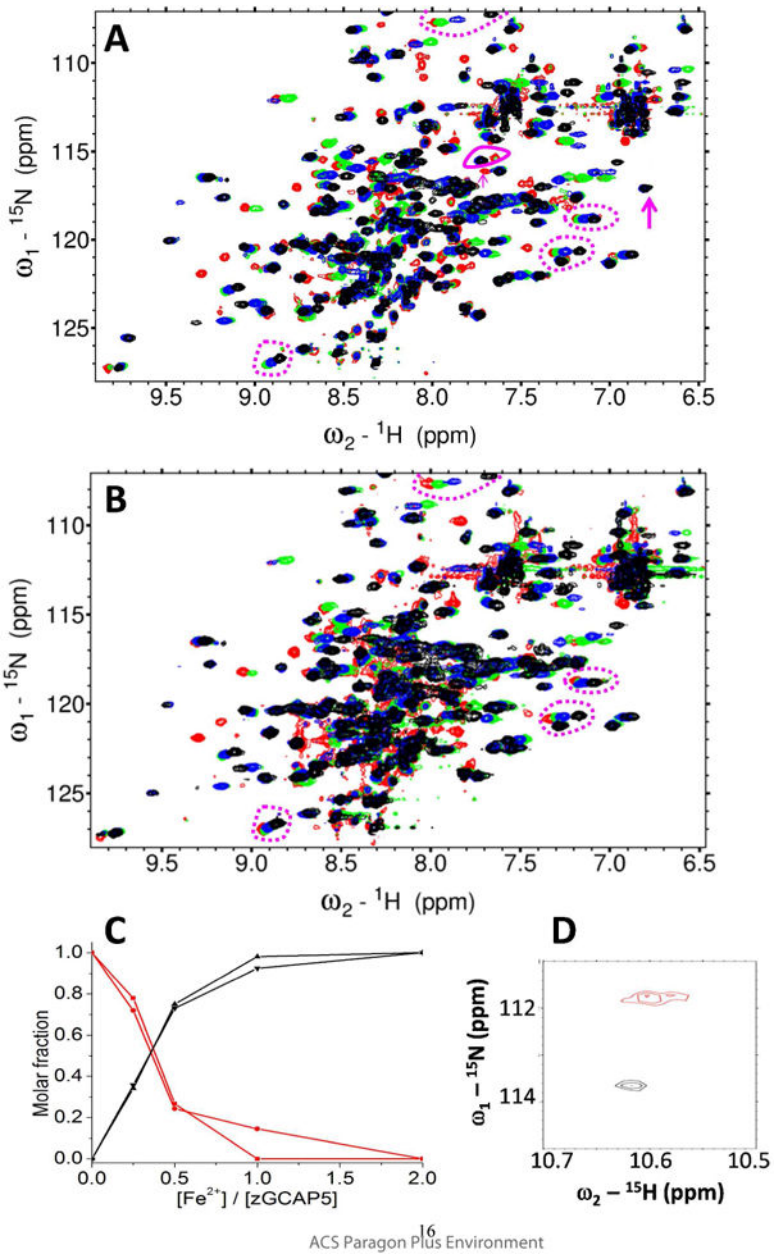

Figure 4. NMR titration of Fe^{2+} binding to GCAP5

Overlay of ^{1}H-^{15}N HSQC spectra of ^{15}N-labeled GCAP5^{WT} (A) or GCAP5$^{C15A/C17A}$ (B) titrated with 0 (red), 0.50 (green), 1.0 (blue), and 3 (black) equivalents of Fe^{2+} ions. Peaks exhibiting slow exchange kinetics during the titration are marked by magenta arrows and solid circle in panel A, and are not present in the titration of GCAP5$^{C15A/C17A}$ (B). The slow exchange peaks at 7.6/115 and 7.7/116 ppm in the Fe^{2+}-free GCAP5^{WT} spectrum are tentatively assigned to Cys15 and Cys17 because these peaks are abolished in the spectrum of Fe^{2+}-free GCAP5$^{C15A/C17A}$. The slow exchange peaks at 7.7/115 and 6.8/117 ppm in the Fe^{2+}-bound GCAP5^{WT} spectrum are also assigned to Cys15 and Cys17 because these peaks are abolished in the spectrum of Fe^{2+}-bound GCAP5$^{C15A/C17A}$. Representative peaks exhibiting fast exchange kinetics are marked by the magenta dashed circles in panels A and

B. (C) NMR intensity of the slow exchange peaks from Fe^{2+}-free state (7.6/115 and 7.7/116 ppm, red) and Fe^{2+}-bound state (7.7/115 and 6.8/117 ppm, black) are plotted as a function of Fe^{2+} concentration. (D) Expanded view of downfield region of HSQC spectrum of $GCAP5^{C15A/C17A}$. The downfield peak at 10.60/111.8 ppm, assigned to Gly68 in EF2 in the Fe^{2+}-free state (red), is shifted to 10.65/113.8 ppm in the Fe^{2+}-bound state (black), suggesting that Fe^{2+} may bind to EF2.

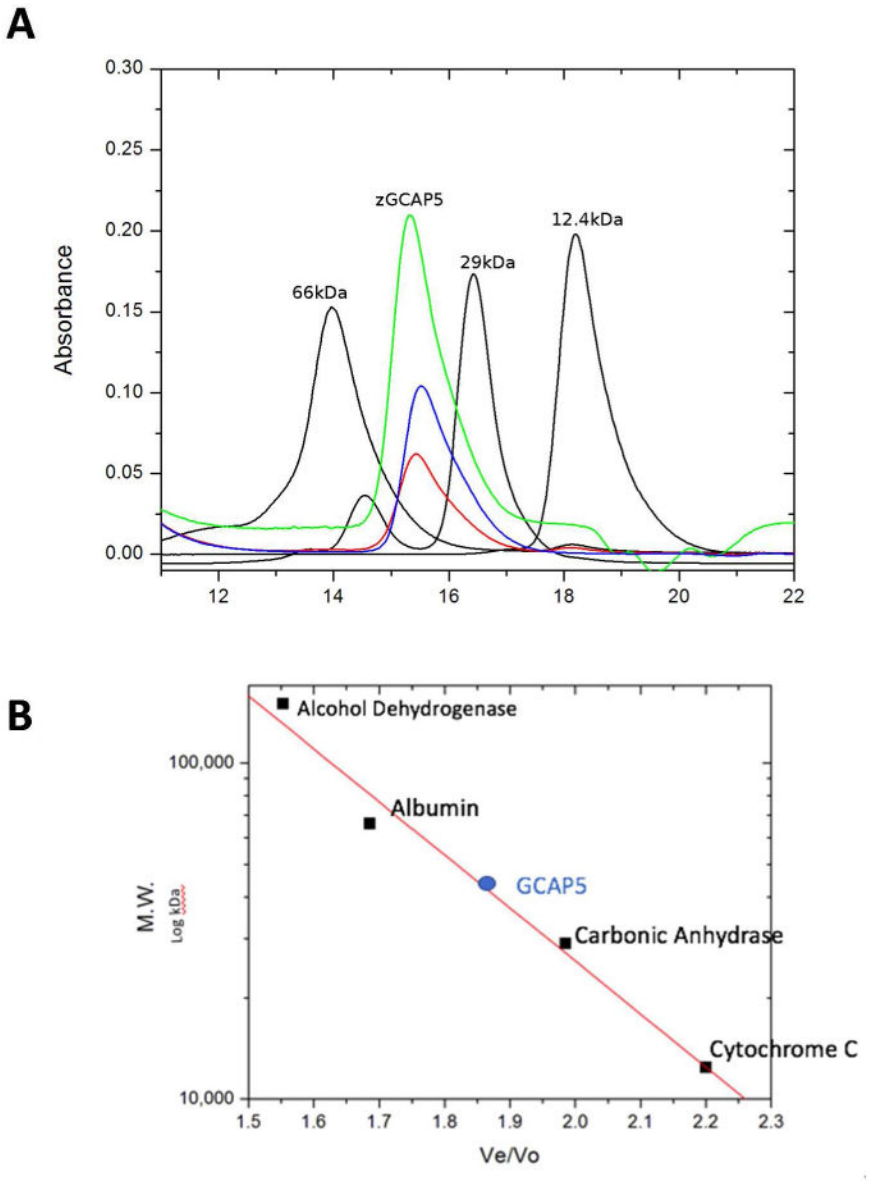

Figure 5. GCAP5 is a dimer

(A) SEC chromatograms of $GCAP5^{WT}$ in the presence of Mg^{2+} (green) and Fe^{2+} (blue), and $GCAP5^{C15A/C17A}$ in the presence of Fe^{2+} (red). SEC chromatograms of protein standards (12.4, 29, and 66 kDa) are shown in black. (B) Molar mass calibration curve. The molar mass of GCAP5 was calculated to be 42 kDa (based on the protein standard masses), consistent with GCAP5 forming a dimer in both Fe^{2+}-free and Fe^{2+}-bound states.

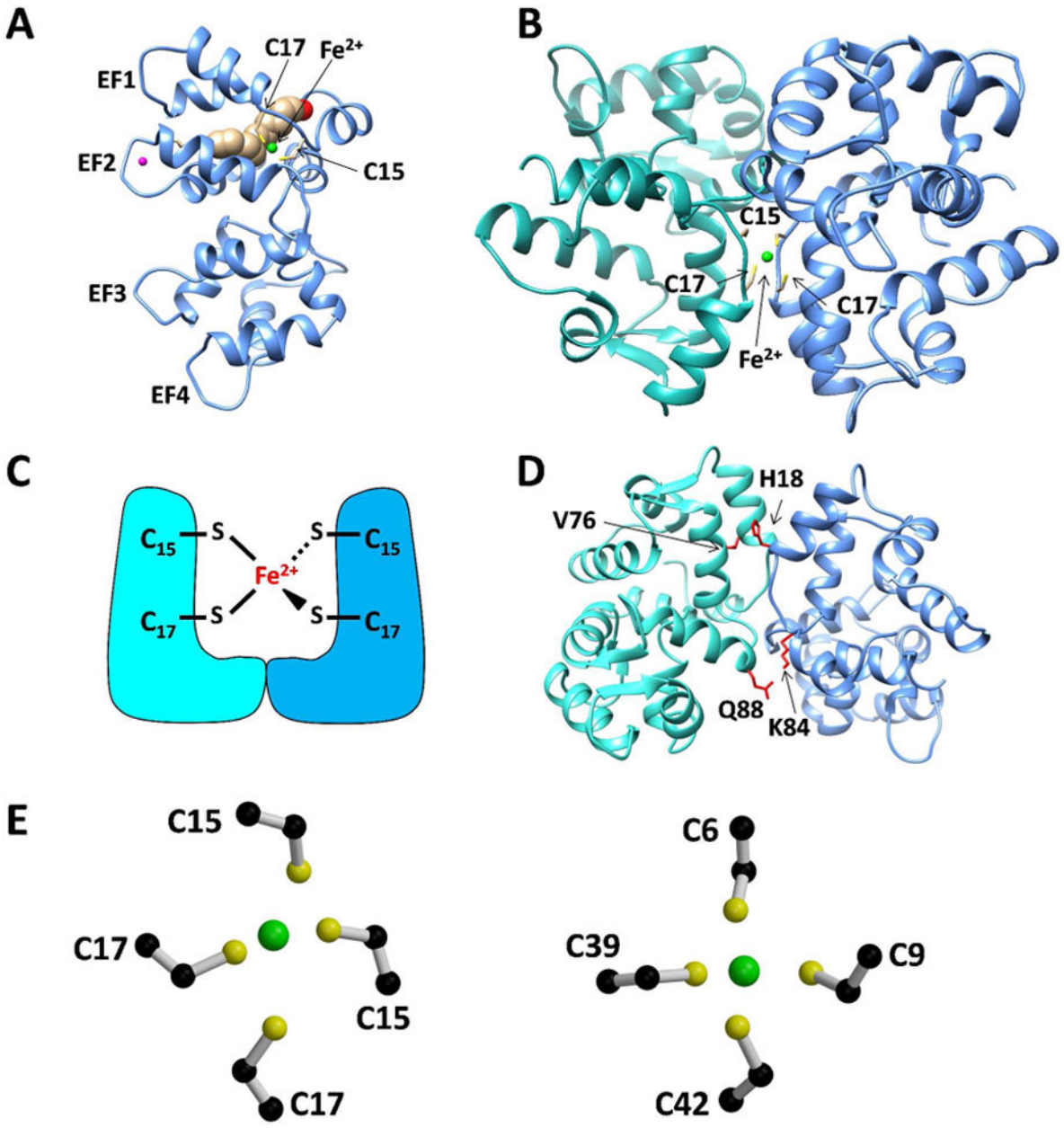

Figure 6. Structural model of GCAP5 bound to Fe^{2+}

(A) Homology model structure of Ca^{2+}-free/Mg^{2+}-bound GCAP5 with bound Fe^{2+} (green) ligated by Cys15 and Cys17 (yellow). Mg^{2+} bound to EF2 (magenta) is supported by the downfield NMR resonance assigned to Gly68 in EF2 of Mg^{2+}-bound GCAP5 (Fig. S2), which is similar to that observed for Mg^{2+}-bound GCAP1[17]. Covalently attached myristic acid is depicted by a space-filling model (brown). (B) Docked structure of GCAP5 dimer in a $[Fe(SCys)_4]$ complex. (C) Schematic model of GCAP5 dimer showing Fe^{2+} bound to residues Cys15 and Cys17. (D) Intermolecular residue contacts at the GCAP5 dimer interface. The H18 imidazole group interacts with side-chain methyl groups of V76, and K84 side-chain amine group is hydrogen bonded to the side-chain carbonyl group of Q88.

(E) Close-up view of Fe^{2+} binding site in GCAP5 (left) compared to that of rubredoxin (1FMH, right). Carbon, sulfur, and Fe^{2+} atoms are colored black, yellow, and green.

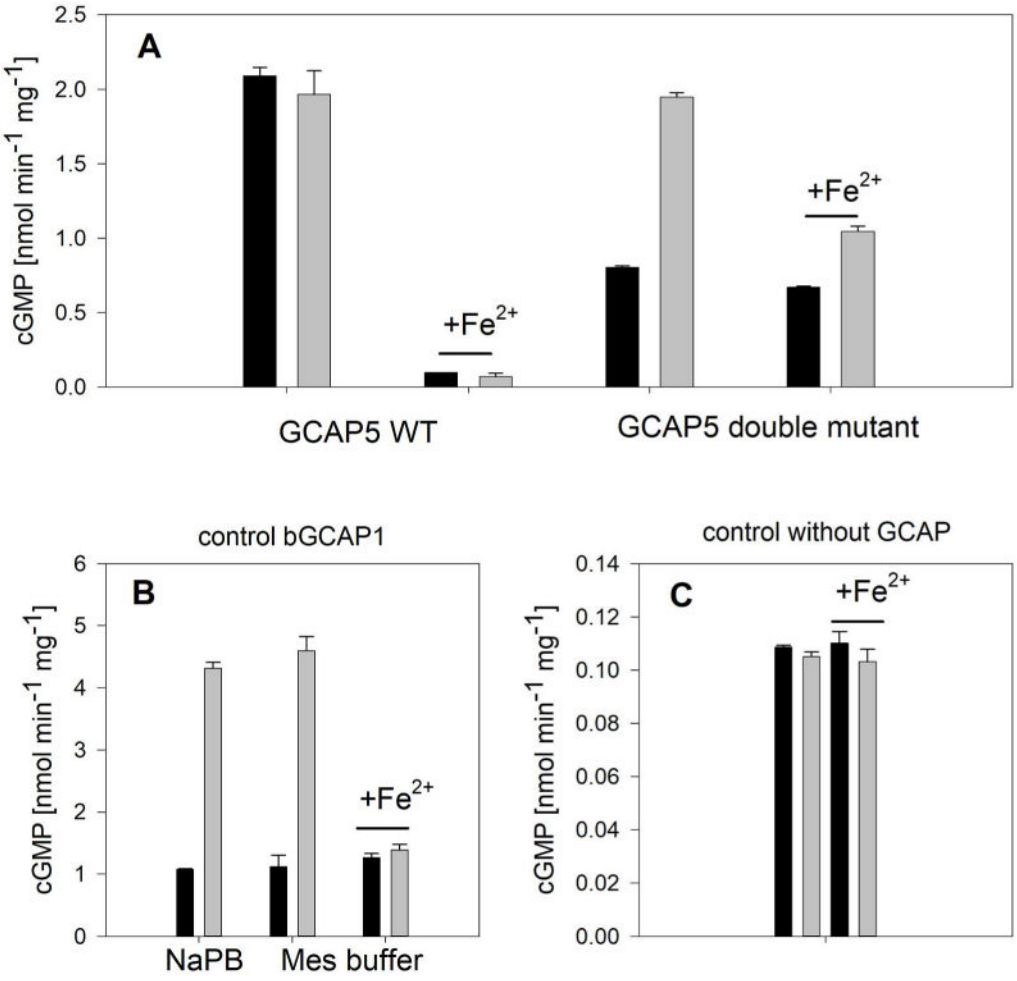

Figure 7. GC-E enzyme activity regulated by GCAPs in the presence of Fe^{2+}

(A) Activation of recombinant human GC-E by wildtype (WT) GCAP5 or the C15A/C17A double mutant. GCAP concentration was 10 μM, black bars are incubations in the presence of 1.5 μM free [Ca^{2+}], gray bars are in the presence of Ca^{2+}-chelating EGTA (< 10 nM). Fe^{2+} was present at 100 nM. (B) Control incubations of human recombinant GC-E with 5 μM bovine GCAP1 in the absence and presence of 100 nM Fe^{2+}. Lyophilized GCAP1 was either resuspended in Na-phosphate buffer (NaPB) or in Mes buffer like GCAP5. (C) Control incubation of GC-E without GCAPs in the presence and absence of Ca^{2+} and/or Fe^{2+}. Basal activity showed no influence of either Ca^{2+} or Fe^{2+}. Black and gray bars in (B) and (C) are as indicated in (A).